Dalton Transactions

ROYAL SOCIETY OF CHEMISTRY

PAPER

View Article Online
View Journal | View Issue

Cite this: *Dalton Trans.*, 2023, **52**, 3176

Experimental and computational investigation of heteroatom substitution in nucleolytic Cu(II) cyclen complexes for balancing stability and redox activity†

Jan Hormann,[a] Olga Verbitsky,[b] Xiaoyu Zhou,[c] Beatrice Battistella,[a,d] Margarete van der Meer,[a] Biprajit Sarkar,[a,e] Cunyuan Zhao*[c] and Nora Kulak*[a,b]

Cu(II) complexes of cyclen-based ligands Cu**L**^{1}–Cu**L**^{6} were synthesized and characterized. The corresponding ligands **L**^{1}–**L**^{6} comprise different donor sets including S and O atoms. Whereas cyclen (**L**^{1}) is commercially available, **L**^{2}–**L**^{6} were synthesized according to protocols available in the literature. Cleavage activity of the complexes towards plasmid DNA was tested in the presence and absence of ascorbate as a reducing agent (oxidative *vs.* hydrolytic cleavage). As previously shown, the substitution of N donor atoms with hard donor O atoms leads to efficient oxidative nucleases, but dissociation of the complex upon reduction. We thus opted for S substitution (soft donors) to stabilize the reduced Cu(I) species. Increasing the S content, however, leads to species that are difficult to reoxidize in order to ensure efficient oxidative DNA cleavage. We are showing by experimental (cyclic voltammetry) and computational means (DFT) that the rational combination of O and S atoms next to two nitrogen donors within the macrocycle (oxathiacyclen complex Cu**L**^{6}) leads to the stabilization of both redox states. The complex thus exhibits the highest oxidative DNA cleavage activity within this family of cyclen-based Cu(II) complexes – without leaching of the metal ion during reduction.

Received 11th October 2022,
Accepted 14th January 2023

DOI: 10.1039/d2dt03284h

rsc.li/dalton

Introduction

Metal complexes of cyclen (1,4,7,10-tetraazacyclododecane) and of the smaller analog 1,4,7-triazacyclononane have been successfully applied in the hydrolytic cleavage of DNA and RNA, with the aim of developing agents for biotechnological purposes.[1–5] The oxidative cleavage of DNA by such macrocyclic copper complexes has been investigated less extensively,[6–8] despite their potential use as anticancer agents. In cell studies various nucleolytic copper complexes have shown high activity against cancer cells.[9–11]

There are several approaches to increase the cleavage activity of cyclen metal complexes towards nucleic acids: multinuclear complexes,[12–14] attachment of nucleobase-affine moieties[15] or positively charged groups for better interaction with the phosphate backbone.[16]

Whereas the 4N donor ligand cyclen has been frequently applied in such studies, heteroatom-substituted analogs are less common. This might be due to difficult synthetic accessibility to the derivatives, whereas cyclen itself is commercially available. By using analogous precursor molecules, however, their syntheses are equally straightforward.

Older and recent examples of macrocyclic ligands with different heteroatoms have focused on the larger analog cyclam (1,4,8,11-tetraazatetradecane), *e.g.* the Cu(I) and Cu(II) complexes of the *trans*-dithiacyclam derivative have been suggested as analogs of blue copper proteins and copper monooxygenases,[17–19] and its Cu(II) complex with two molecules of diclofenac, a nonsteroidal anti-inflammatory drug

[a]*Institut für Chemie und Biochemie, Freie Universität Berlin, Fabeckstr. 34/36, 14195 Berlin, Germany*
[b]*Institut für Chemie, Otto-von-Guericke-Universität, Magdeburg, Universitätsplatz 2, 39106 Magdeburg, Germany. E-mail: nora.kulak@ovgu.de*
[c]*MOE Key Laboratory of Bioinorganic and Synthetic Chemistry, School of Chemistry, Sun Yat-Sen University, XinGang Rd. W., Guangzhou 510275, China. E-mail: ceszhcy@mail.sysu.edu.cn*
[d]*Department of Chemistry, Humboldt Universität zu Berlin, Brook-Taylor-Str. 2, 12489 Berlin, Germany*
[e]*Institut für Anorganische Chemie, Universität Stuttgart, Pfaffenwaldring 55, 70569 Stuttgart, Germany*

†Electronic supplementary information (ESI) available: Synthesis of ligands and complexes, UV/VIS and EPR spectroscopy, X-ray crystallography, summary of stability constants, quench and BNPP assay, intrinsic reaction coordinates, structural parameters and cartesian coordinates of optimized structures. Crystallographic data for [Cu**L**^{3}(NO_3)]NO_3 (CIF). CCDC 1569176. For ESI and crystallographic data in CIF or other electronic format see DOI: **https://doi.org/10.1039/d2dt03284h**

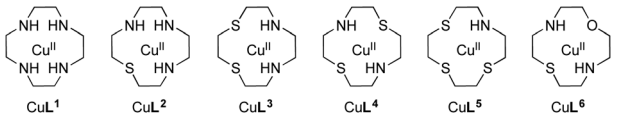

Fig. 1 Cu(II) complexes containing the macrocyclic ligands $\mathbf{L^1}$–$\mathbf{L^6}$ studied in the present work.

(NSAID) at the axial positions, has been used to generate reactive oxygen species (ROS) for killing breast cancer cells and highly resistant breast cancer stem cells.[20]

In the last couple of years, we have systematically investigated the coordination chemistry and electrochemical properties of Cu(II) cyclen derivatives substituted with one sulfur or one and more oxygen donors.[6,7] To find out if exchanging nitrogen donors in Cu(II) cyclen [Cu([12]aneN$_4$)] (Cu$\mathbf{L^1}$) with several sulfur atoms also had an effect on nuclease activity, Cu$\mathbf{L^2}$–Cu$\mathbf{L^5}$ were prepared and their DNA cleavage activity was compared to that of Cu$\mathbf{L^1}$. Additionally, Cu$\mathbf{L^6}$ having an O donor as well as an S donor merged in the macrocyclic ligand $\mathbf{L^6}$, was synthesized (Fig. 1). Based on our previous findings, an heteroatom exchange N → O/S was expected to have a significant impact on the redox potential and DNA cleavage activity of the respective complexes.[6,7]

We studied the redox chemistry, oxidative and hydrolytic DNA cleavage activity of the Cu(II) complexes Cu$\mathbf{L^1}$–Cu$\mathbf{L^6}$ and rationalized their nucleolytic activity with computational results by DFT.

Results and discussion

Synthesis and characterization of ligands and complexes

Ligand syntheses. All ligands, except for $\mathbf{L^1}$, which was commercially available, were synthesized in multistep organic syntheses. $\mathbf{L^2}$, 1-thia-4,7,10-triazacyclododecane or [12]aneN$_3$S, was synthesized according to a procedure previously published by our group.[6] Ligand $\mathbf{L^3}$, 1,4-dithia-7,10-diazacyclododecane or [12]aneN$_2$S$_2$, was synthesized in a three-step procedure according to the literature[21] (ESI, S-1†): *N*,*N*′-(ethane-1,2-diyl) bis(2-chloroacetamide) was reacted with ethanedithiol to give a dilactame. In contrast to the synthesis of analogous oxacyclen derivatives,[7] chlorinated starting materials were used in this procedure instead of tosylated ones. This procedure allowed a smooth reduction step for the dilactame instead of a harsh detosylation reaction, usually resulting in low yields.

Ligand $\mathbf{L^4}$, 1,7-dithia-4,10-diazacyclododecane or [12]aneNSNS, was synthesized according to the literature[22] in a four-step procedure over a dilactame (ESI, S-1†): In contrast to the synthesis of the regioisomeric compound $\mathbf{L^3}$ ([12]aneN$_2$S$_2$), where a dichlorinated amide and a dithiol were used to form the dilactame, cyclization happened in the case of $\mathbf{L^4}$ by reaction of thioethers of an acid chloride and a diamine. The amine was used in excess in order to trap the released hydrogen chloride. Reduction of the dilactame lead to the desired compound.

Ligand $\mathbf{L^5}$, 1,4,7-trithia-10-azacyclododecane or [12]aneNS$_3$, was synthesized according to the same protocol[21] as $\mathbf{L^3}$ (ESI, S-1†): Therefore, 2,2′-thiodiethanethiol was cyclized with a chlorinated diamine under high-dilution conditions in the presence of cesium carbonate.

Ligand $\mathbf{L^6}$, 1-oxa-7-thia-4,10-diazacyclododecane, shortly [12]aneNONS or oxathiacyclen, was synthesized according to a procedure published by Hambley *et al.* comprising the cyclization of tosylated precursors[23] with slight modifications (ESI, S-1†).

Complex syntheses. Complexes Cu$\mathbf{L^1}$ and Cu$\mathbf{L^2}$ were synthesized according to a protocol previously published by our group.[6] Cu$\mathbf{L^3}$, Cu$\mathbf{L^4}$, and Cu$\mathbf{L^5}$ were synthesized by mixing a ligand solution with an equimolar copper(II) nitrate solution using methanol, ethanol or acetonitrile, respectively, as a solvent. For Cu$\mathbf{L^6}$, ethanol was employed, and the ligand was freshly sublimed prior to the complexation reaction (ESI, S-1†).

The synthesis of the Cu(II) complex of the commercially available cyclic thioether 1,4,7,10-tetrathiacyclododecane was tried by mixing the methanolic solutions of ligand and copper (II) nitrate. However, elemental analysis of the obtained light-blue product revealed the formation of a Cu(I) species of unknown composition. As shown in Table S-4 (ESI†), the stability constant ($\log K$) of the Cu(II) complex is 3.4, whereas the stability constant of the corresponding Cu(I) species is 12.9.[24] Since all other complexes were used with copper in oxidation state +II, no attempt was made to further characterize this Cu(I) species. Indeed, it has been reported in the literature that N_2S_2 donor sets in macrocyclic ligands (here, *cis*-/*trans*-dithiacyclen) can accommodate the cupric as well as cuprous state, whereas the former is preferred for a N_4 donor set, and the latter for an S_4 donor set.[17]

Complexes Cu$\mathbf{L^1}$–Cu$\mathbf{L^6}$ were characterized by elemental analysis, UV/VIS, IR and EPR spectroscopy as well as ESI mass spectrometry (ESI, S-1 and S-2†).

UV/VIS spectroscopy. The UV/VIS spectra showed the typical d–d transitions in the region 600–660 nm (ESI, Fig. S-2.1 and Table S-2†). A red shift and sharp increase of the extinction coefficient was observed as the number of sulfur atoms increased. This can be attributed to the ligand-to-metal charge transfer (LMCT) S → Cu(II). Due to the more expanded orbitals S is a better donor than O in LMCT.[25]

IR spectroscopy. In the IR spectra of complexes Cu$\mathbf{L^1}$–Cu$\mathbf{L^6}$ (ESI, Fig. S-2.2a–f†), indication for ionic (nitrate counterion, ν_{as} 1320–1380 cm^{-1} (NO_2 asymmetric stretching), ρ 800–825 cm^{-1} (NO_2 deformation)) as well as coordinated nitrate (nitrato ligand, ν_{as} 1410–1440 cm^{-1} and ν_s 1290–1330 cm^{-1} (NO_2 asymmetric and symmetric stretching), ν 960–980 cm^{-1} (N–O stretching)) can be found. By comparison with the literature[26,27] it can be derived that the nitrato ligand is bound to the Cu(II) center in a monodentate fashion *via* one of the oxygen atoms (η^1), suggesting a composition [Cu$\mathbf{L}$(O-NO$_2$)]NO$_3$ for $\mathbf{L}$ = $\mathbf{L^1}$–$\mathbf{L^6}$.

X-ray crystallography. More detailed structural information was derived from single crystal X-ray diffraction. Whereas the molecular structures of complexes [Cu$\mathbf{L^1}$(NO$_3$)]NO$_3$ and

$[CuL^2(NO_3)]NO_3$ in the solid state have been described earlier in the literature,[6,28] the structures of CuL^3–CuL^6 remain unknown in the literature. For complex CuL^3 and CuL^6, it was possible to obtain crystals suitable for X-ray analysis by slow diffusion of diethyl ether into a saturated methanolic solution of the complex. The quality of the obtained data set was not good enough in case of CuL^6, however, the data were used as an input for the computational studies (*vide infra*).

In Fig. 2, the molecular structure of complex CuL^3 in the solid state is shown. The crystallographic data of the complex can be found in the ESI (S-3),† whereas selected bond lengths and angles can be found in Table 1.

Complex CuL^3, like CuL^1 and CuL^2,[6,28] consists of a $[CuLNO_3]^+$ cation and a non-coordinating nitrate anion. Due to the small ring size of the cyclen derivatives, a square planar coordination is not possible – in contrast to the cyclam analogs,[17,18] but complexes CuL^1–CuL^3 rather exhibit a distorted square pyramidal coordination. The base of the pyramid is provided by the macrocyclic heteroatoms and the edge of the pyramid by an oxygen atom of the nitrate ligand. The Cu–N bond length is approximately 2 Å (as in CuL^1 and CuL^2), whereas the Cu–S bond lengths are elongated (*ca.* 2.3 Å) due to the larger covalent radius of sulfur (this corresponds to the value observed for CuL^2).[6] The nitrate ligand coordinates in a η^1 fashion as it does in complexes CuL^1 and CuL^2, and as suggested by IR spectroscopy (*vide supra*). In CuL^3, the bond length between the Cu^{2+} ion and O(1), the top of the pyramid, is 2.11 Å, and it is little larger for CuL^2 (2.16) and CuL^1 (2.18). Thus, the structures of the cyclen complex CuL^1 and its analogs with one and two sulfur donors, respectively, are very similar. Any effects on the reactivity based on the solid state structures can thus be excluded for these three complexes.

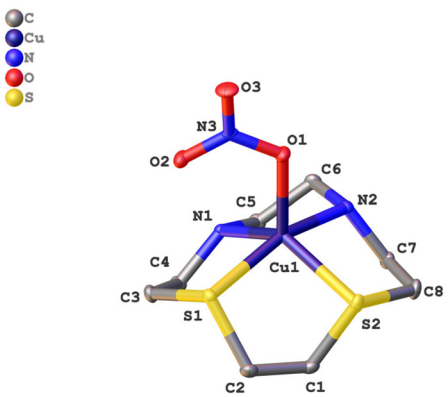

Fig. 2 Molecular structure of $[CuL^3(NO_3)]NO_3$ in the solid state. For clarity reasons the hydrogen atoms and the nitrate counterion have been omitted.

Table 1 Selected bond lengths and angles of complex $[CuL^3(NO_3)]NO_3$

	Bond length [Å]		Bond angle [°]
Cu(1)–O(1)	2.105	S(1)–Cu(1)–O(1)	101.396
Cu(1)–S(2)	2.353	S(2)–Cu(1)–O(1)	108.179
Cu(1)–S(1)	2.349	N(1)–Cu(1)–O(1)	113.141
Cu(1)–N(1)	2.025	N(2)–Cu(1)–(O1)	97.379
Cu(1)–N(2)	2.007	S(1)–Cu(1)–S(2)	85.740
C(1)–C(2)	1.525	S(2)–Cu(1)–N(1)	138.655
O(1)–N(3)	1.285	S(1)–Cu(1)–N(2)	161.194
		N(1)–Cu(1)–N(2)	86.051

DNA cleavage

Hydrolytic DNA cleavage. DNA cleavage without the addition of an external reducing agent was conducted to test for hydrolytic cleavage activity under approximate physiological conditions at 37 °C in Tris-HCl buffer (pH 7.4). Agarose gel electrophoresis (1% agarose) was used to monitor the conversion of supercoiled (I) pBR322 DNA into its nicked (II) and linear (III) form. While the compact form I migrates the fastest through the pores of the gel, the open-circular form II is the slowest, and form III appears in between the latter forms on the gel. Experiments were carried out at least three times in order to generate reliable data with standard deviation. pBR322 supercoiled plasmid DNA was incubated with complexes CuL^1–CuL^6 for 24 h. A tenfold concentration (0.4 mM, Fig. 3) was used with respect to the experiments in the presence of ascorbate (*cf.* Fig. 5) due to the expected lower activity during hydrolysis reactions.[7] Even after 24 h, however, cleavage activity was not significantly increased when compared to the background reaction ("control" in Fig. 3).

The hydrolysis of the phosphate ester bonds in the small DNA model molecule BNPP (bis(4-nitrophenyl)phosphate) was investigated for comparison, here exemplarily with CuL^2 and CuL^6 (Fig. 4). The release of the hydrolysis product *p*-nitrophenolate was detected by UV/VIS spectroscopy for the latter compound but not for the former, even after 8 d incubation. Even CuL^6 showed poor reactivity, since the cleavage product was only observed in the spectrum after 48 h (ESI, Fig. S-6.1†), and doubling the concentration (2 mM instead of 1 mM) did not show a significant effect (ESI, Fig. S-6.2†).

Oxidative DNA cleavage. Oxidative cleavage of pBR322 plasmid DNA by complexes CuL^1–CuL^6 was studied in the

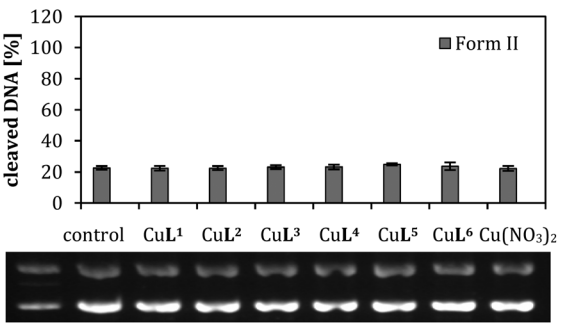

Fig. 3 Cleavage activities of complexes CuL^1–CuL^6 and $Cu(NO_3)_2$ (0.4 mM) on pBR322 plasmid DNA (0.025 μg μL^{-1}) in Tris-HCl buffer (50 mM, pH 7.4) at 37 °C for 24 h. Illustrated is the average of three experiments, the standard deviations are shown as error bars.

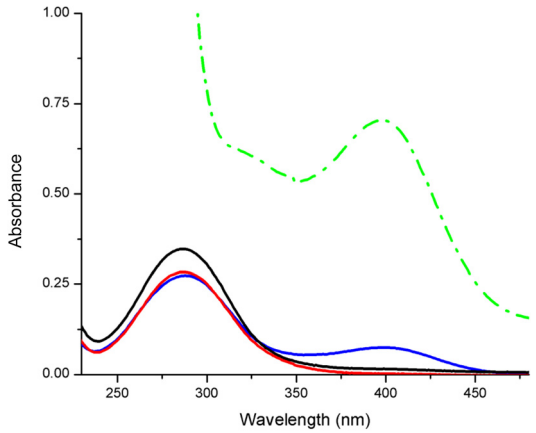

Fig. 4 UV/Vis spectra of BNPP (0.08 mM) in the absence (black line) and presence of complexes Cu**L**^{2} (1 mM, red line), Cu**L**^{6} (1 mM, blue line) and phosphodiesterase (0.05 U, green line), respectively, in 50 mM Tris-HCl buffer (pH 7.5) after an incubation of 8 d (only 2 d for phosphodiesterase) at 37 °C for monitoring the formation of the BNPP cleavage product *p*-nitrophenol (λ_{max} = 400 nm). The absorbance of the complexes was subtracted.

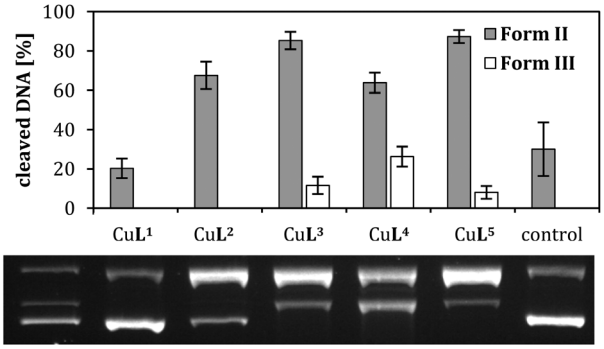

Fig. 5 Cleavage activities of complexes Cu**L**^{1}–Cu**L**^{5} (0.04 mM) on pBR322 plasmid DNA (0.025 μg μL^{-1}) in Tris-HCl buffer (50 mM, pH 7.4) and ascorbic acid (0.32 mM) at 37 °C for 2 h. Illustrated is the average of three experiments with standard deviations shown as error bars (top) and a representative agarose gel (bottom).

presence of ascorbic acid as a reducing agent (0.32 mM, similar to its intracellular concentration). A comparison of the cleavage activity of the complexes Cu**L**^{1}–Cu**L**^{5} is shown in Fig. 5.‡ The exchange of one nitrogen atom by one sulfur atom from [Cu([12]aneN$_4$)] Cu**L**^{1} to [Cu([12]aneN$_3$S)] Cu**L**^{2} leads to a triplication of cleavage activity as previously reported by our group.[6] Additional increase of the sulfur content in the ligand further enhances the cleavage activity: Complex Cu**L**^{3} [Cu([12]aneN$_2$S$_2$)] entirely cleaves form I DNA and even generates a small amount of form III DNA. While complex Cu**L**^{5} [Cu([12]aneNS$_3$)] has a similar cleavage activity, the regioisomer of Cu**L**^{3}, Cu**L**^{4} [Cu([12]aneNSNS)], shows the highest cleavage

‡Cleavage activity of the metal salt alone, Cu(NO$_3$)$_2$ is shown in Fig. S-5.1.† Its activity is comparable to the weaker DNA cleaving agents in this study like Cu**L**^{2}.

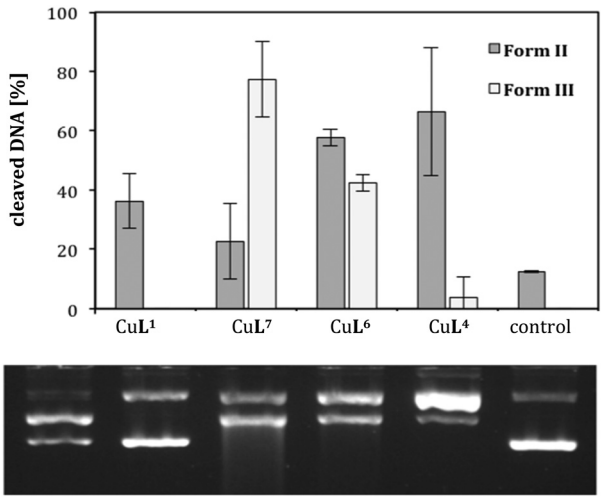

Fig. 6 Cleavage activities of complexes Cu**L**^{1}, Cu**L**^{4}, Cu**L**^{6} and Cu**L**^{7} (**L**^{7} = 1,7-dioxacyclen)[7] (0.04 mM) on pBR322 plasmid DNA (0.025 μg μL^{-1}) in Tris-HCl buffer (50 mM, pH 7.4) and ascorbic acid (0.32 mM) at 37 °C for 2 h. Illustrated is the average of three experiments with standard deviations shown as error bars (top) and a representative agarose gel (bottom).

activity among the complexes Cu**L**^{1}–Cu**L**^{5}. Intriguingly, in the case of dithiacyclen, the *trans* regioisomer of dithiacyclen is more active than the *cis* form, in contrast to the corresponding dioxacyclen analogs, where the *cis* regioisomer presented the highest reactivity.[7] In the latter case, the leaching of Cu ions from the ligand with too hard donor atoms for Cu(I), does not allow a correlation between redox chemistry and DNA cleavage activity, whereas in the current work for Cu**L**^{3} and Cu**L**^{4} it is indeed possible (*vide infra*). Above that, for Cu**L**^{3}, its tendency to form inactive, dimeric species should be considered.[17]

A comparison of Cu**L**^{1}, Cu**L**^{4} and Cu**L**^{6}, *i.e.* the complexes of the parent compound cyclen, the *trans*-dithiacyclen and *trans*-oxathiacyclen, with Cu**L**^{7} (**L**^{7} = *trans*-dioxacyclen[7]), is shown in Fig. 6. The order in the diagram is chosen such that the oxygen content in the macrocycle is decreasing from left to the right (dioxacyclen > oxathiacyclen > dithiacyclen), also corresponding to a decrease in DNA cleavage activity. The dioxacyclen complex Cu**L**^{7} generated up to 80% form III DNA, whereas dithiacyclen Cu**L**^{4}, the most active species among the sulfur-containing cyclen analogs (Fig. 5), only generated 10% form III DNA.§ Cu**L**^{6}, representing a hybrid of the oxacyclen[7] and thiacyclen series, concordantly exhibits cleavage activity between that of the dioxa and the dithia analog.

§It should be mentioned that a comparison of Fig. 5 and 6 reveals different cleavage activities for the complexes Cu**L**^{1} and Cu**L**^{4}. It has to be considered, that a direct comparison between different gel sets is not possible, but only within one single gel set. This can also be derived from the observation that the amount of form II in different batches of plasmid DNA (*cf.* controls) and the lengths of error bars can be distinct from each other in different gel sets (here, Fig. 5 and 6). This is why we avoid comparison of cleavage activities obtained in different gel experiments in our discussion.

Furthermore, it should be mentioned that, despite the employed Tris buffer is a potential competitive ligand for Cu(II), the stability constants of the complexes under study are higher than the one for the Cu(II)-tris system[29] (5.3–6.3 *vs.* >8, *cf.* ESI, S-4†). Nevertheless, the large excess of Tris (approx. 100-fold and 1000-fold in the hydrolytic and oxidative cleavage reactions, respectively) in the experiments suggests that the macrocyclic ligands and Tris could compete for Cu(II) and/or form ternary complexes. Experiments with a non-interfering buffer, MOPS (ESI, Fig. S-5.1 and S-5.2,† direct comparison TRIS/MOPS) gave comparable results, and thus indicate that DNA cleavage is not initiated by other Cu(II) species than Cu**L**^{1}–Cu**L**^{6}. As expected from the Pearson's principle, the stability of the Cu(II) complexes decreases with increasing sulfur content of the macrocycle, whereas the stability of the respective Cu(I) complexes increases (ESI, Table S-4†). Since an efficient switching of the oxidation state is decisive for oxidative DNA cleavage, it is required for both the Cu(II) and the Cu(I) species to be sufficiently stable. This is indeed the case for Cu**L**^{3} and Cu**L**^{4}.

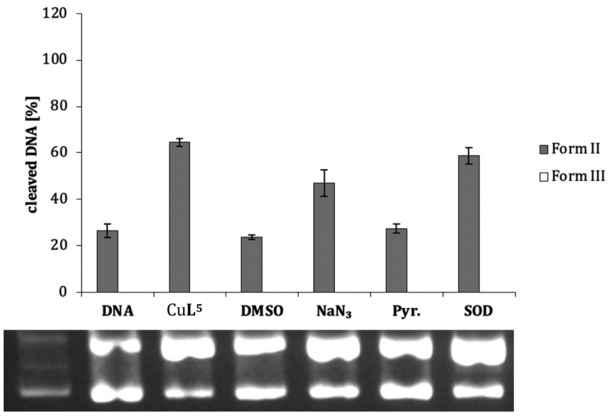

Fig. 7 Cleavage activities of complex Cu**L**^{5} (0.04 mM) on pBR322 plasmid DNA (0.025 μg μL^{-1}) in Tris-HCl buffer (50 mM, pH 7.4), PBS (1.25×) and ascorbic acid (0.32 mM) at 37 °C for 2 h in the presence of the indicated ROS scavengers. Illustrated is the average of three experiments, the standard deviations are shown as error bars (top) and a representative agarose gel (bottom).

Investigation of redox chemistry

Detection of reactive oxygen species. "Free" Cu(II) as well as Cu(II) complexes are known to form reactive oxygen species (ROS) in the presence of a reducing agent by redox cycling between the oxidation state Cu(II) and Cu(I).[30] To further identify the species that are involved in the case of complexes Cu**L**^{1}–Cu**L**^{6}, incubation for DNA cleavage was conducted in the presence of scavengers for ROS like hydroxyl radicals (DMSO),[31] singlet oxygen (NaN_3),[32] hydrogen peroxide (pyruvic acid)[33] and superoxide (superoxide dismutase, SOD)[32] and compared to the cleavage without any scavenger.

As shown exemplarily for complex Cu**L**^{5} in Fig. 7, pyruvate (Pyr.) and DMSO exert a significant inhibition effect on DNA cleavage. This is the case also for most of the other complexes (ESI, Table S-5 and Fig. S-5.3–S-5.8†), suggesting the presence of peroxo species and hydroxyl radicals during DNA cleavage (except for Cu**L**^{1}, with very low cleavage activity anyway). An oxidative cleavage mechanism can thus be assumed, where the detected ROS attack the DNA base or ribose moieties and cause degradation of this biomolecule.[34]

In order to exclude, that potential interactions between Cu(II) and the quencher molecules have an impact on the results, ROS were additionally detected *via* a fluorescence assay. Herein, fluorogenic compounds, terepthtalate (TPA) and pentafluorobenzenesulfonyl fluorescein (PBSF), get activated in the presence of hydroxyl radicals and hydrogen peroxide,[35,36] respectively (ESI, Fig. S-5.9 and S-5.10,† exemplarily for Cu**L**^{5}). Both ROS were detected, corroborating the results of the quenching studies using agarose gel electrophoresis.

EPR spectroscopy. EPR spectra of Cu**L**^{1} and Cu**L**^{4} were measured at pH 7.4 in the absence and presence of ascorbic acid (ESI, Fig. S-2.3 and S-2.4†). Whereas the EPR spectrum of the cyclen complex Cu**L**^{1} did not change after addition of ascorbic acid (ESI, Fig. S-2.3a,† and neither did the color of the complex solution), the *trans*-dithiacyclen complex Cu**L**^{4} showed a significantly changed spectrum accompanied by a color change from blue to light green 30 min after addition of ascorbic acid: two different Cu(II) species can be observed which are overlapping at around g = 2.00. When the simulated values for Cu**L**^{4} are compared before and after addition of ascorbic acid (ESI, Fig. S-2.4d†), "species 1" can be attributed to Cu**L**^{4} (35% of the complex have not reacted). Since the measurement before/after addition was done with the same solution, the measurement before the addition can be used as a reference for EPR quantification. It can thus be concluded that the spin quantity is half after addition of ascorbate (ESI, Fig. S-2.4e†), which suggests the formation of a diamagnetic species (50%, *cf.* computational studies, dimerization tendency) next to paramagnetic species (50%, of which 35% is remaining Cu**L**^{4}, and 65% can be attributed to a new species with a different structure than before).

Cyclic voltammetry. Whereas the cyclic voltammogram of Cu**L**^{1} and previously studied oxacyclen complexes show electrochemically irreversible one-electron reduction at −1.0 to −0.5 V,[6,7] the voltammograms of complexes Cu**L**^{2}–Cu**L**^{6} exhibit reversible one-electron reduction waves, which can be attributed to the reduction of Cu(II) to Cu(I) (Fig. 8, peak-to-peak separation ΔE_p around 60 mV and ratio of peak currents i_{pa}/i_{pc} close to 1). Even after repeated redox cycles no "free" copper species ($E_{1/2}$ = −0.57 V vs. FcH/FcH^+ under the same measurement conditions[6]) were detected as in the case of cyclen and oxacyclen derivatives[6] (Fig. 8 right, exemplarily for Cu**L**^{3}). The respective half-wave potentials are listed in Table 2.

The irreversibility of reduction might be due to the low stability of Cu(I) in cyclen and oxacyclen complexes, whereas a high stability of Cu**L**^{2}–Cu**L**^{5} in their +I and +II oxidation states is assumed (*cf.* ESI, Table S-4†).

Relationship between redox properties and oxidative DNA cleavage activity. The reduction potentials can be correlated

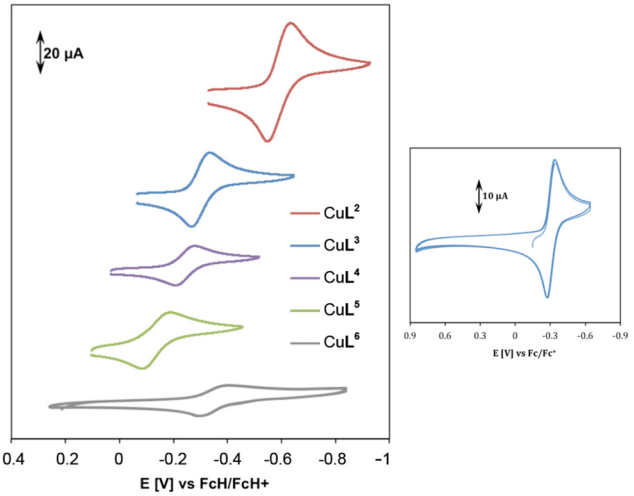

Fig. 8 Cyclic voltammetry of complexes CuL^2–CuL^6 in 0.1 M KCl solution at 100 mV s^{-1} and room temperature (left). Multiple scanning for complex CuL^3 at the same conditions (right).

Table 2 $E_{1/2}$ values of complexes CuL^2–CuL^6 *vs.* FcH/FcH^+ (0.1 M KCl)

	$E_{1/2}$ [V]
CuL^2	−0.60
CuL^3	−0.31
CuL^4	−0.23
CuL^5	−0.14
CuL^6	−0.35

with the DNA cleavage activity of complexes CuL^2–CuL^5:¶ CuL^2 exhibits a half-wave potential $E_{1/2}$ of −0.6 V *vs.* FcH/FcH^+, whereas $E_{1/2}$ of the regioisomeric dithia-substituted complexes CuL^3 and CuL^4, the most efficient oxidative DNA cleaving agents within this series, are only a half and a third, respectively, of $E_{1/2}(CuL^2)$. Those complexes can thus be easily reduced to the respective Cu(I) species, which is necessary to generate the ROS. Re-oxidation to Cu(II) while forming ROS in the sense of a catalytic reaction is feasible with complexes $Cu(I)L^3$ and $Cu(I)L^4$ due to their fast reaction with O_2.[37]

The *cis*-dithiacyclen complex CuL^3 showing more negative $E_{1/2}$ indicates higher stability for oxidation state +II in comparison to *trans*-dithiacyclen complex CuL^4, which is reflected in the higher oxidative DNA cleavage activity of the latter compound (Fig. 5), *i.e.* easier formation of ROS due to Cu(I) generation, but also in the stability constants for the Cu(II) species (ESI, Table S-4,† $\log K(CuL^3) \approx 14$ *vs.* $\log K(CuL^4) \approx 12$).[17]

$E_{1/2}$ is only −0.14 V *vs.* FcH/FcH^+ for CuL^5, thus it should be more easily reduced and a more efficient oxidative nuclease than CuL^2–CuL^4. Nevertheless, CuL^5 was shown to be as active as CuL^3. It can be assumed that the Cu(I) complex of L^5 is more stable than the respective Cu(II) species (ESI, Table S-4†). The re-oxidation to a Cu(II) species might therefore be thermodynamically less favorable, rendering ROS generation less probable in the case of complex CuL^5 in comparison to *e.g.* CuL^4, where Cu(I) and Cu(II) species are equally stable (ESI, Table S-4†).

CuL^6 exhibits a completely reversible reduction with a half-wave potential of −0.35 V (Table 2 and Fig. 8), an intermediate value with regard to ease of reduction. Concerning DNA cleavage activity, this complex is, however, much more active than CuL^2–CuL^5, which might be due to its low dimerization tendency in the cuprous state (*vide infra*, computational studies). Cu(II) oxathiacyclen CuL^6 as a hybrid between Cu(II) *trans*-dithiacyclen CuL^4 and Cu(II) *trans*-dioxacyclen CuL^7, showed DNA cleavage activity which is in between the other two complexes (Fig. 6). Whereas the S atom promotes the Cu(I) stabilization, the O atom favors the Cu(II) oxidation state. The presence of both, S and O donor provides the right balance for Cu(II) reduction and Cu(I) reoxidation, facilitating the switch between the redox states Cu(II) and Cu(I), and thus ensuring efficient ROS generation.[38] Consequently, CuL^7, which shows the highest cleavage activity, comes with the disadvantage of not being able to stabilize Cu(I), so that copper ions can leach from the ligand and might be responsible for the DNA cleavage instead of the assumed complex. For the oxygen-containing macrocycles, as reported earlier,[7] an increase in the number of oxygen atoms promotes metal reduction, but at the same time the affinity of the ligand to Cu(I) decreases. This problem was circumvented within this work by the use of the here presented thiacyclen and oxathiacyclen Cu(II) complexes.

Computational studies and comparison with experimental results

There are some theoretical studies concerning the cleavage of DNA or RNA in the literature by metal complexes,[39–42] however, not touching on the here presented compounds.

In order to better understand the chemical reactivity of CuL^1 –CuL^6 regarding hydrolytic and oxidative DNA cleavage, density functional theory (DFT) was used as a complementary method next to the experimental ones. The complexes were studied regarding their dimerization tendency and redox potential. The pK_a values of metal-coordinated water molecules ($M–OH_2$) were predicted as well were the reaction mechanisms of the formation of ROS and the BNPP hydrolysis theoretically investigated.

Dimerization tendency. The formation of dimers might play a role for the reactivity of the complexes in hydrolytic as well as oxidative cleavage reactions. Indeed, the dimerization product of mononuclear copper complexes is usually considered to be responsible for catalytic deactivation. To get an insight into dimerization tendencies, the formation free energies of dimeric μ-hydroxido-bridged and double-bridged μ-hydroxido Cu(II) complexes (Fig. 9a) as well as μ-hydroxido-bridged Cu(I) complexes (Fig. 9b) were calculated. As shown in

¶Any effects should be discussed against the background of the fact, that the reduction of oxygen by Cu(I) is an inner-sphere process, whereas the electrochemical reduction represents an outer-sphere process,[58] thus DNA cleavage activity does not necessarily correlate with reduction potentials.

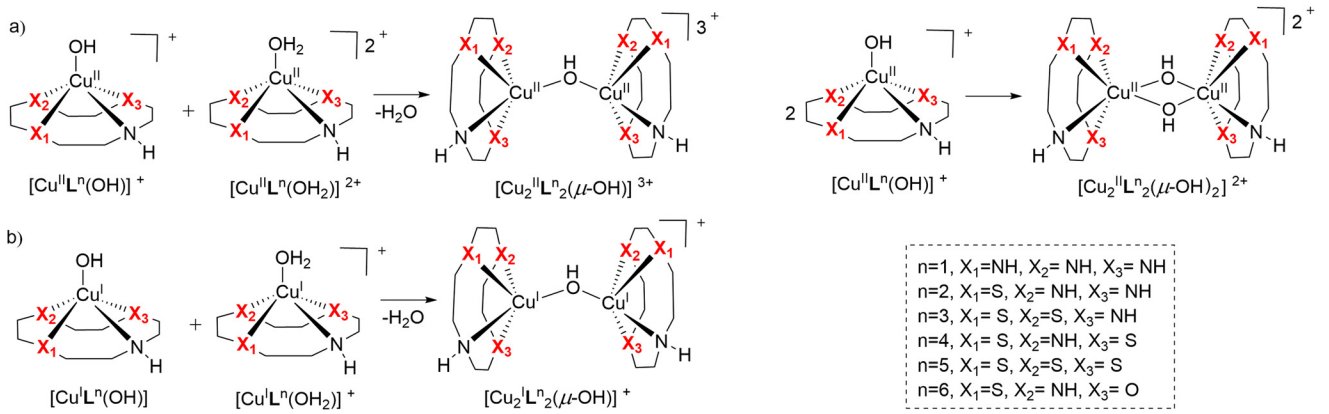

Fig. 9 Dimerization schemes of (a) Cu(II)$\mathbf{L}^n$ complexes and (b) Cu(I)$\mathbf{L}^n$ complexes.

Table 3 Formation free energies (in kcal mol^{-1}) of dimeric Cu(II) complexes along with their Cu(I) analogs

Structure	$[Cu^{II}_2\mathbf{L}^1{}_2(\mu\text{-OH})]^{3+}$	$[Cu^{II}_2\mathbf{L}^2{}_2(\mu\text{-OH})]^{3+}$	$[Cu^{II}_2\mathbf{L}^3{}_2(\mu\text{-OH})]^{3+}$	$[Cu^{II}_2\mathbf{L}^4{}_2(\mu\text{-OH})]^{3+}$	$[Cu^{II}_2\mathbf{L}^5{}_2(\mu\text{-OH})]^{3+}$	$[Cu^{II}_2\mathbf{L}^6{}_2(\mu\text{-OH})]^{3+}$
ΔG_f	−74.7	−12.2	19.0	57.7	−11.3	−6.1
Structure	$[Cu^{II}_2\mathbf{L}^1{}_2(\mu\text{-OH})_2]^{2+}$	$[Cu^{II}_2\mathbf{L}^2{}_2(\mu\text{-OH})_2]^{2+}$	$[Cu^{II}_2\mathbf{L}^3{}_2(\mu\text{-OH})_2]^{2+}$	$[Cu^{II}_2\mathbf{L}^4{}_2(\mu\text{-OH})_2]^{2+}$	$[Cu^{II}_2\mathbf{L}^5{}_2(\mu\text{-OH})_2]^{2+}$	$[Cu^{II}_2\mathbf{L}^6{}_2(\mu\text{-OH})_2]^{2+}$
ΔG_f	−66.7	−13.1	−27.7	−14.9	−36.9	−14.7
Structure	$[Cu^{I}_2\mathbf{L}^1{}_2(\mu\text{-OH})]^{+}$	$[Cu^{I}_2\mathbf{L}^2{}_2(\mu\text{-OH})]^{+}$	$[Cu^{I}_2\mathbf{L}^3{}_2(\mu\text{-OH})]^{+}$	$[Cu^{I}_2\mathbf{L}^4{}_2(\mu\text{-OH})]^{+}$	$[Cu^{I}_2\mathbf{L}^5{}_2(\mu\text{-OH})]^{+}$	$[Cu^{I}_2\mathbf{L}^6{}_2(\mu\text{-OH})]^{+}$
ΔG_f	−11.1	−13.1	−11.7	−11.3	−12.2	−3.5

Fig. 9, the $[Cu^{II}_2\mathbf{L}^n{}_2(\mu\text{-OH})]^{3+}$ complex with mono μ-hydroxido bridge is formed by the dimerization of $[Cu^{II}\mathbf{L}^n(OH)]^+$ and $[Cu^{II}\mathbf{L}^n(OH)_2]^{2+}$ complexes, and the dimerization of $[Cu^{II}\mathbf{L}^n(OH)]^+$ complexes result in double-bridged μ-hydroxido $[Cu^{II}_2\mathbf{L}^n{}_2(\mu\text{-OH})_2]^{2+}$ complexes. Likewise, the dimerization of $[Cu^{I}\mathbf{L}^n(OH)]$ and $[Cu^{I}\mathbf{L}^n(OH)_2]^+$ complexes yields the mono μ-hydroxido bridged $[Cu^{I}_2(\mathbf{L}^n)_2(\mu\text{-OH})]^+$ complex.

It can be derived from Table 3 that the double-bridged μ-hydroxido complexes $[Cu^{II}_2\mathbf{L}^n{}_2(\mu\text{-OH})_2]^{2+}$ (n = 1–6) are in general more stable than their mono-bridged counterparts ($\Delta G_f < 0$). The dimerization process is the easiest in case of Cu(II)$\mathbf{L}^1$ reflected in the most negative ΔG_f. This indicates that the low reactivity of Cu(II)$\mathbf{L}^1$ in plasmid DNA degradation might be due to dimer formation.[6] The most reactive complex, $Cu^{II}\mathbf{L}^6$, concordantly exhibits the least negative value, indicating low stability of its dinuclear complex, and explaining its activity in the BNPP hydrolysis reaction (Fig. 4).

For $Cu^{I}\mathbf{L}^n$ (n = 1–5), the $[Cu^{I}_2\mathbf{L}^n{}_2(\mu\text{-OH})]^+$ complexes all have ΔG_f values in the range of −11 to −13 kcal mol^{-1}. These values are more negative than the ΔG_f value of the $[Cu^{I}_2\mathbf{L}^6{}_2(\mu\text{-OH})]^+$ species, again suggesting the least stable dimer for the $Cu^{I}\mathbf{L}^6$ analog. This result is consistent with $Cu^{II}\mathbf{L}^6$ being the most active oxidative cleaving agent within the series, since formation of $Cu^{I}\mathbf{L}^6$ and ROS is decisive for this process, which could be hindered by any dimerization side reaction.

Reduction potentials. The one-electron reduction potentials were calculated employing eqn (1) and (2) deduced from the Born–Haber cycle of the redox process[43] (see Fig. 10a).

$$\Delta G^{\circ,\mathrm{redox}}_{\mathrm{solv}} = \Delta G^{\circ\mathrm{redox}}_{\mathrm{g}} + \Delta G^{\circ}_{\mathrm{s}}(\mathrm{Red}) - \Delta G^{\circ}_{\mathrm{s}}(\mathrm{Ox}) \quad (1)$$

$$E^{\circ}_{\mathrm{calc}} = -\Delta G^{\circ,\mathrm{redox}}_{\mathrm{solv}}/F \quad (2)$$

As demonstrated in Fig. 10b, the reduction potentials of the six complexes follow the order CuL^5 > CuL^3 > CuL^4 > CuL^6 >

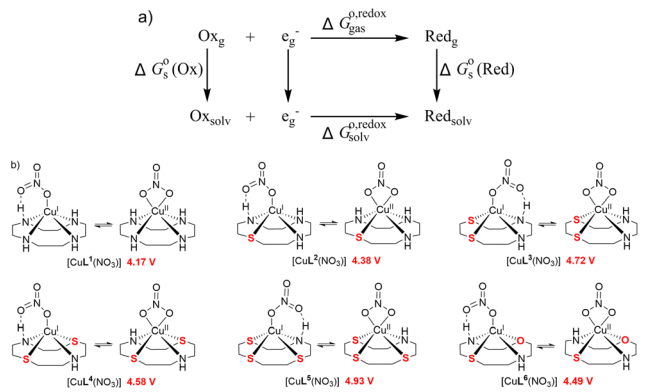

Fig. 10 (a) Thermodynamic Born–Haber cycle of the redox processes, (b) structural variations during the redox processes and corresponding redox potentials for $Cu^{I/II}\mathbf{L}^n$ (in red).

CuL^2 > CuL^1. The higher reduction potential of CuL^n (n = 3–5) indicates easier reduction from the Cu(II) complexes to the Cu(I) analogs. This correlates well with the experimental electrochemical results, where CuL^5 > CuL^4 > CuL^3 > CuL^6 > CuL^2 was found for the half-wave potentials, *i.e.* only CuL^4 and CuL^3 are switched, when the two rows are compared. As indicated for the cyclic voltammetric studies, the trends are reflected in the oxidative cleavage activity of the complexes with CuL^6 representing an exception (highest cleavage activity despite of intermediate values for $E_{1/2}$, however, low dimerization tendency, *vide supra*).

Mechanism for ROS generation. Regarding the formation of ROS, a mechanism for the reaction with dioxygen is proposed (Fig. 11a), and the corresponding optimized structures are shown in Fig. 11b. According to the structural features, the complexes CuL^n can be divided into two types: one type has two N atoms *trans* to each other coordinated to the copper center (n = 1, 2, 4 and 6); the other type (n = 3, 5) has a heteroatom (O or S) *trans* to an N atom coordinating to the copper center. In the reactant n-O-RC (n = 1–6 corresponding to complexes of ligands L^1–L^6), the axial coordination site of the Cu(I) center is occupied by a water molecule, and also a crucial hydrogen bond is formed between the metal-coordinated water molecule and the oxygen molecule. The Cu–O_{water} bond length is 2.21, 2.20, 2.20 and 2.17 Å, respectively, for CuL^n (n = 1, 2, 4 and 6). The distance between the Cu atom and the O atom of the oxygen molecule is with 4.42, 4.64, 4.72 and 4.64 Å, respectively, significantly longer than the Cu–O_{water} bond.

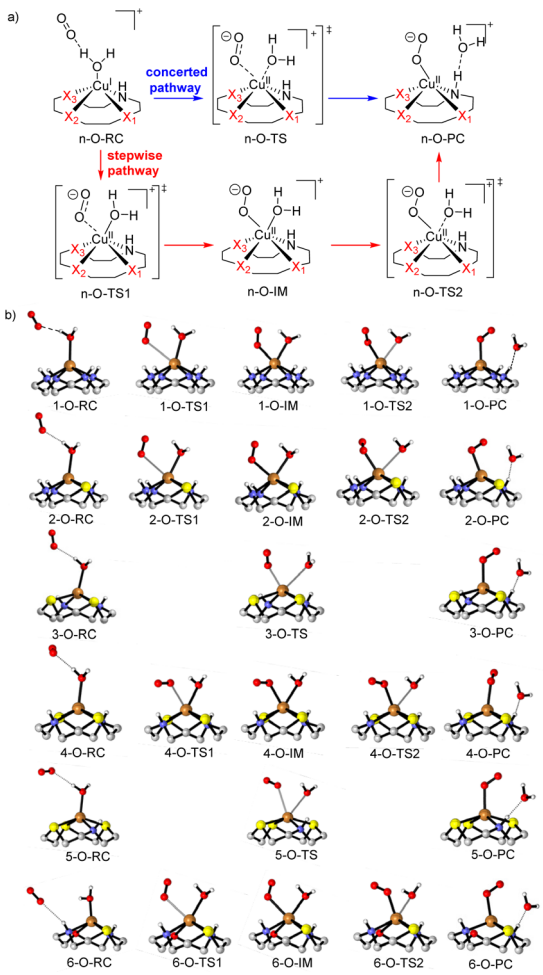

Fig. 11 (a) Proposed reaction mechanism of the generation of ROS, (b) optimized complex structures.

Because of the different structures resulting from heteroatom substitution in the cyclen moiety, different mechanisms of the generation of ROS are proposed. For CuL^n (n = 1, 2, 4 and 6), complexes with two N atoms in *trans* position coordinated to the copper center, the mechanism is believed to be a stepwise pathway as depicted in Fig. 11a in red. In the transition state n-O-TS1, it is noted that the copper center is attached to the nucleophilic oxygen molecule. The distance of the Cu–O_{oxygen} decrease to 2.93, 2.76, 2.47 and 2.51 Å for n-O-TS1 (n = 1, 2, 4 and 6), respectively. The Cu–O_{oxygen} distances become even smaller in the intermediate n-O-IM. In n-O-IM, the coordination sphere of the copper center consists of two strong O donors (the metal-coordinated oxygen molecule and the water molecule), one strong N-donor and three X_n donors from the cyclen. The bond length of the Cu–O_{oxygen} is 2.14, 2.16, 2.19 and 2.27 Å for n-O-IM (n = 1, 2, 4 and 6), respectively. The Cu–O coordinated combination of the Cu(II) center with the water molecule is further weakened in the n-O-TS2, and the Cu–O_{oxygen} bond is more strengthened. Subsequently, the water molecule is dissociated from the Cu(II) center in n-O-PC. However, for the CuL^3 and CuL^5 complexes, only one transition state was discovered in the generation of ROS, which suggests a concerted pathway (see Fig. 11a in blue). In the transition state n-O-TS (n = 3 and 5, for intrinsic reactions coordinates *cf.* ESI, Fig. S-7†), it could be seen that O_{water} and one of the O atoms of the oxygen molecule coordinate to the copper center. The Cu–O_{water} distance is 2.73 and 2.98 Å, and the Cu–O_{oxygen} distance is 2.27 and 2.78 Å for 3-O-TS and 5-O-TS, respectively. A tendency for the cleavage of the Cu–O_{water} bond and simultaneous formation of a Cu–O_{oxygen} bond is observed upon going from n-O-RC to n-O-TS (n = 3 and 5). At last, a superoxide radical anion ($O_2^{\bullet-}$) ROS is formed in a metal-bonded manner in the n-O-PC state. All optimized structural parameters are reported in the ESI (ESI, Table S-7.1†).

The calculated relative free energy profiles for the generation of ROS by the CuL^n complexes are shown in Fig. 12. It can be established that the nucleophilic attack of the oxygen molecule to the copper center should be the rate-determining step for the CuL^n (n = 1, 2, 4 and 6) complexes. A comparison between CuL^1, CuL^2 and CuL^6 reveals that the relative free energy of the CuL^2 complex is the highest (1.7 kcal mol^{-1} in liquid phase), which can be ascribed to the lower electronegativity of the sulfur donor and thus weaker Lewis acidity of the copper center. Moreover, the energy barriers for the CuL^n (n = 3, 4 and 5) complexes are higher compared to the CuL^n complexes (n = 1, 2 and 6) due to an increase of the sulfur

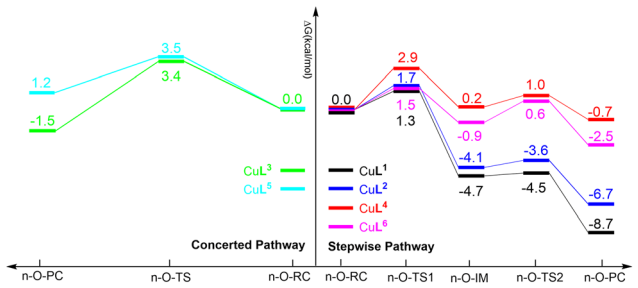

Fig. 12 Relative free energy profiles for the generation of ROS by Cu**L**^{n} complexes in liquid phase: Cu**L**^{n} (n = 1, 2, 4 and 6) complexes through a stepwise mechanism and Cu**L**^{n} (n = 3 and 5) complexes through a concerted mechanism.

content and an even more distinct reduction of the Lewis acidity of the copper center.

According to the above presented data for dimerization tendencies and the reduction potential, the higher reduction potential of Cu^{I}**L**^{6} complex compared to Cu^{I}**L**^{1} and Cu^{I}**L**^{2} is considered to be a more important factor in the oxidative cleavage of DNA than the dimerization tendency since the free energy barriers for ROS generation are similar for all above-mentioned complexes.

Also, the lower free energy barrier of Cu^{I}**L**^{4} compared to Cu^{I}**L**^{3} and Cu^{I}**L**^{5} is more favorable in the oxidative cleavage of DNA. Therefore, the Cu^{I}**L**^{6} complex is expected to be the most efficient DNA oxidative cleaving agent, followed by Cu^{I}**L**^{4}. This is confirmed by the experimental data.

pK_a values. Similarly to the redox process, the pK_a values of the metal-coordinated water molecules were deduced from a Born–Haber cycle (Fig. 13a). Eqn (3) was used to infer the values from the Born–Haber cycle of the deprotonation processes.[44,45]

$$pK_a = \frac{[\Delta G_g + \Delta G_s(A^-) + \Delta G_s(H^+) - \Delta G_s(AH)]}{2.303RT} \quad (3)$$

The pK_a values of the metal-coordinated water molecules of all the structures of interest are summarized in Fig. 13b. The calculated pK_a values of $[Cu^{II}\mathbf{L}^n(OH_2)]^{2+}$ (n = 1–3) systems were

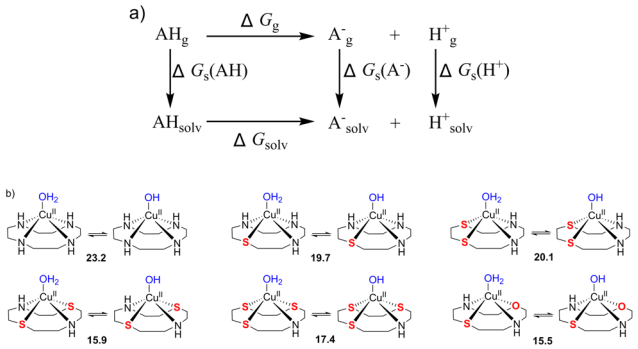

Fig. 13 (a) Thermodynamic Born–Haber cycle of the deprotonation processes, (b) the structural variations during deprotonation processes and the calculated pK_a values for complexes Cu**L**^{1}–Cu**L**^{6}.

close to each other, while a lower M–OH_2 pK_a was observed for the other three complexes (n = 4–6), which is favorable for the formation of the M–OH nucleophile. This trends can be corroborated with the BNPP cleavage experiment, where Cu**L**^{6} represents a much better catalyst for phosphoester cleavage than Cu**L**^{2} (Fig. 4).

Conclusions

Six different Cu(II) complexes of heteroatom-substituted cyclen ligands were synthesized and characterized, among them four new compounds. Their cleavage activity towards plasmid DNA was tested twofold. Under hydrolytic conditions, Cu**L**^{1}–Cu**L**^{6} were not able to cut DNA within 24 h. We have shown here that relatively low pK_a values for their aqua complexes as well as low dimerization tendencies can explain this observation. Under oxidative conditions (reduction of Cu(II) by ascorbate leading to ROS formation) Cu**L**^{6} was most efficient followed by Cu**L**^{4}, Cu**L**^{5} and Cu**L**^{3} with regioisomeric diathiacyclen ligands (Cu**L**^{3} and Cu**L**^{4}) forming equally stable Cu(II) and Cu(I) complexes and a trithiacyclen ligand (Cu**L**^{5}). The latter one might hinder a reoxidation to Cu(II) due to strong stabilization of the Cu(I) species.

Compared to the previously reported oxygen-rich analogs,[7] DNA cleavage efficiency is slightly decreased. However, the redox processes of the sulfur-rich and the mixed sulfur/oxygen analogs triggers Cu^{II}/Cu^{I} redox process reversibility due to higher stability of the corresponding Cu(I) species, which is of fundamental importance for the ROS generation.

Therefore, Cu**L**^{6} represents the most interesting candidate within this series. The presence of an oxygen donor (stabilizing Cu(II)) as well as an sulfur donor (stabilizing Cu(I)) next to two nitrogen donors within the ligand scaffold, can strike a balance between the two effects, which the pure thia- or oxa-derivatives suffer from. On the one hand, if the Cu(I) state is too stable, as in sulfur-rich systems, the reoxidation, and thus the ROS formation is inhibited. On the other hand, an oxygen-rich system leads to the release of the copper ion once it is reduced to Cu(I) due to its low affinity to O donors.[6,7] Cu**L**^{6} thus represents a compromise between a set of hard (O) and soft donor atoms (S) next to intermediate donor atoms (N) for stabilizing the hard and soft Lewis acids, respectively, Cu(II) and Cu(I). This concept is also used in nature by redox-active blue copper proteins, for instance azurin, however, only with N and S donors.[46]

Our approach of combining experimental and theoretical data for the evaluation of Cu(II) metallonucleases, and the observed correlation between these data, shows that rational design for this class of biologically active molecules is possible. Decisive parameters like dimerization tendencies, reduction potentials (for oxidative DNA cleavage) and pK_a values (for hydrolytic DNA cleavage) can be estimated before elaborate experiments are carried out. We hope this work inspires other groups in the field to use a combinatory approach of theoretical and experimental studies to identify metal complexes being worthwhile to synthesize.

Experimental section

Materials and methods

All chemical reagents were purchased from Sigma–Aldrich if not stated otherwise. Only HPLC-grade solvents were used.

UV/VIS absorption spectra were recorded with a Varian Cary 100 spectrophotometer by using precision cells made of quartz (1 cm) at 25 °C.

Fluorescence experiments were carried out at room temperature in Tris and in MOPS buffer (50 mM, pH 7.4). Hydroxyl radicals and hydrogen peroxide were detected by means of the fluorogenic sensors TPA (50 μM) and PBSF (25 μM), respectively. The solutions were composed of Tris (or MOPS) buffer (50 mM, pH 7.4), sensor, L-ascorbic acid (0.25 mM), scavenger compounds (DMSO (400 mM) when using TPA or pyruvate (2 mM) when using PBSF) and Cu(II) complex or Cu(II) salt (40 μM). Samples were incubated at room temperature for 2.5 h and fluorescence spectra were recorded in the range of 350–550 nm (λ_{ex} = 320 nm) for TPA-containing samples and 490–600 nm (λ_{ex} = 485 nm) for PBSF-containing samples (slit width 5 nm). Fluorescence spectra were measured in 1000 μL (for TPA) and 500 μL (for PBSF) quartz fluorescence cuvettes with an Agilent Cary Eclipse fluorescence spectrometer the photomultiplier voltage adjusted to 780 V and 720 V using TPA and PBSF, respectively.

Electrospray mass spectra were obtained in positive-ion mode by using an Agilent 6210 ESI-TOF mass spectrometer.

Elemental analyses were performed by using a Vario EL elemental analyzer.

IR spectra were measured with a Nicolet™ iS™ 5 FT-IR spectrometer (Thermo Fisher). The measurement was performed directly from the solid sample without prior preparation.

X-ray diffraction data were collected with a Bruker-AXS SMART CCD system. The structures were solved by direct methods and refined by full-matrix least-squares methods (SHELX-97). CCDC 1569176 (Cu**L**^{3}) contains the supplementary crystallographic data for this paper.†

Cyclic voltammetry experiments were carried out in an aqueous 0.1 M KCl solution. Millipore water was used to prepare the solutions. The water was degassed before by bubbling dinitrogen into it. A three-electrode configuration (glassy carbon working electrode, Pt counter electrode, Ag wire as pseudo-reference) and a PAR VersaSTAT 4 potentiostat were used. The ferrocene/ferrocenium (FcH/FcH^{+}) couple served as internal reference. Due to the poor solubility of ferrocene in water, ferrocene was dissolved in acetonitrile (6.7 mM) and added to the solution after each measurement. The measurement was then repeated to allow for referencing to FcH/FcH^{+} (see also ref. 47).

EPR measurements were carried out by the use of a Bruker EMXplus (X band) Spectrometer at an average frequency of 9.35 GHz. The samples have been measured as frozen solutions at an average temperature of 12 K by the use of a liquid Helium-recirculating cryostat (ColdEdge-ER4112HV-CF10-H). Samples have been measured at a power of 2 mW, with an attenuation of 20 dB and modulation amplitude of *ca.* 5 G. EPR simulations were carried out by the use of EasySpin software (version 6.0) supported by Matlab.[59]

Synthesis

All syntheses are described in detail different batches of plasmid D in the ESI (S-1).†

DNA cleavage studies

DNA cleavage activity of complexes Cu**L**^{1}–Cu**L**^{6} towards pBR322 plasmid DNA (Carl Roth) was monitored by agarose gel electrophoresis. All experiments were carried out in triplicate. In a typical experiment, plasmid DNA (0.025 μg mL^{-1}) in Tris-HCl buffer (50 mM, pH 7.4, Fisher Scientific) was mixed with different concentrations of complexes Cu**L**^{1}–Cu**L**^{6} in the presence and absence of ascorbic acid (0.32 mM, Acros). Deionized water (Millipore system) was added up to a total reaction volume of 8 μL before the samples were incubated for a given time. After incubation, samples were analyzed directly or stored at −196 °C (liquid nitrogen) before usage in gel electrophoresis. For analysis, 1.5 μL of loading buffer (containing 3.7 mM bromophenol blue, 1.2 M saccharose in deionized water) was added to the incubation solution and loaded onto an agarose (SeaKem LE, Lonza) gel (1% in 0.5× Tris-borate-EDTA (TBE) buffer, Fisher Scientific) containing ethidium bromide as a staining agent (0.2 μg mL^{-1}, Fisher Scientific). Electrophoresis was carried out at 40 V for 2 h with an electrophoresis unit (Carl Roth; power supply: consort EV243) in 0.5× TBE buffer. Bands were visualized by UV light and photographed by using a gel documentation system (GelDoc, Bio-Rad). The quantity of different DNA forms was estimated by using Image Lab™ software (Bio-Rad). To do so, a value of 1 was assigned to the supercoiled control DNA incubated under the same conditions as in the other experiments but without the addition of metal complexes (labeled "control" or "DNA" in the agarose gels). All other values were expressed relatively to that. Taking into account that the supercoiled form I of plasmid DNA has a smaller affinity towards ethidium bromide, its intensity was afterwards multiplied with a correction factor of 1.22.[48] Small DNA fragments were added together within form III DNA.

To make sure that DNA bands were correctly assigned to forms I, II and III, a DNA ladder was established: 250 μL of pBR322 plasmid DNA (0.025 μg mL^{-1}) were linearized by using EcoRI nuclease, purified by agarose gel electrophoresis and then extracted by using a GenElute™ extraction kit (Sigma–Aldrich). The extract was diluted to 250 μL and mixed with another solution of 250 μL of pBR322 plasmid DNA (0.025 μg mL^{-1}). 2 μL of this solution were loaded into the first pocket of every agarose gel.

Experiments in the presence of ROS scavengers were conducted as described above by using either 200 mM DMSO as hydroxyl radical scavenger, 10 mM NaN_3 as singlet oxygen scavenger, 2 mM pyruvic acid as hydrogen peroxide scavenger or 313 units mL^{-1} superoxide dismutase (SOD, bovine liver, 2000–6000 units mL^{-1}, Sigma–Aldrich) as superoxide radical anion scavenger. Addition of PBS to all samples was necessary, because SOD

was preincubated at 37 °C in 10× PBS for 30 min resulting in a 1.25× PBS concentration in the incubation mixture.

Computational studies

Density functional theory (DFT) using the method of B3LYP function[49,50] was performed in this work, and all the geometry calculations were accomplished with the Gaussian 09 program package.[51] The lanl2dz relativistic effective core potential (ECP) basis[52] was used to describe the metal atom (Cu) and the 6-31+G* basis set for nonmetal atoms (C, H, O, N, P and S) was used in the geometry optimization. The calculations of vibrational frequency and the intrinsic reaction coordinates (IRC)[53,54] were prepared at the same level as above. The vibrational frequency calculation was given to examine the stable point on the potential energy surface. There was no imaginary frequency for the reactants (RCs) and products (PCs) but only one imaginary frequency for the transition states (TSs) at 298.15 K and 1 atm. The IRC was employed to verify the optimal reaction path from RC to PC. Furthermore, to explore accurate energies, single-point energies for all the optimized structures were also studied at the B3LYP/Stuttgart/Dresden (SDD)[55] basis sets with ECP for Cu atoms and 6-311++G** for C, H, O, N, P and S atoms. In addition, solvent effects were investigated by using the SMD[56] continuum model with empirical dispersion correction of GD3[57] (the D3 version of Grimmes dispersion) in water solution (dielectric constant ε = 78.36). All free energies shown were single-point energies in liquid phase.

X-ray crystallographic data for Cu**L**^{2} (CCDC 911568), Cu**L**^{3} (CCDC 1569176)† and Cu**L**^{6} (this work, *vide supra*) were used as initial structures, and the structures of Cu**L**^{1}, Cu**L**^{4} and Cu**L**^{5} were constructed based on the former data.

Conflicts of interest

There are no conflicts to declare.

Acknowledgements

The Studienstiftung des deutschen Volkes is acknowledged for a pre-doctoral fellowship and the Dahlem Research School for a postdoctoral fellowship for J. H. We thank K. Licha for a donation of cyclen and S. Hinojosa and P. Liebing for help with X-ray crystallography. Z. C. Y. gratefully acknowledges the National Natural Science Foundation of China (Grant No. 21573292 and 21773312).

References

1 R. Reichenbach-Klinke and B. König, *J. Chem. Soc., Dalton Trans.*, 2002, 121–130.
2 C. Liu, M. Wang, T. Zhang and H. Sun, *Coord. Chem. Rev.*, 2004, **248**, 147–168.
3 J. R. Morrow and O. Iranzo, *Curr. Opin. Chem. Biol.*, 2004, **8**, 192–200.
4 K. Michaelis and M. Kalesse, *Angew. Chem., Int. Ed.*, 1999, **38**, 2243–2245.
5 T. Joshi, B. Graham and L. Spiccia, *Acc. Chem. Res.*, 2015, **48**, 2366–2379.
6 J. Hormann, C. Perera, N. Deibel, D. Lentz, B. Sarkar and N. Kulak, *Dalton Trans.*, 2013, **42**, 4357–4360.
7 J. Hormann, M. van der Meer, B. Sarkar and N. Kulak, *Eur. J. Inorg. Chem.*, 2015, 4722–4730.
8 C. Wende, C. Lüdtke and N. Kulak, *Eur. J. Inorg. Chem.*, 2014, 2597–2612.
9 S. Tardito and L. Marchiò, *Curr. Med. Chem.*, 2009, **16**, 1325–1348.
10 C. Santini, M. Pellei, V. Gandin, M. Porchia, F. Tisato and C. Marzano, *Chem. Rev.*, 2014, **114**, 815–862.
11 I. Iakovidis, I. Delimaris and S. M. Piperakis, *Mol. Biol. Int.*, 2011, 594529.
12 B. Gruber, E. Kataev, J. Aschenbrenner, S. Stadlbauer and B. König, *J. Am. Chem. Soc.*, 2011, **133**, 20704–20707.
13 A. Bencini, E. Berni, A. Bianchi, C. Giorgi, B. Valtancoli, D. K. Chand and H.-J. Schneider, *Dalton Trans.*, 2003, 793–800.
14 Y.-G. Fang, J. Zhang, S.-Y. Chen, N. Jiang, H.-H. Lin, Y. Zhang and X.-Q. Yu, *Bioorg. Med. Chem.*, 2007, **15**, 696–701.
15 Y. Zhang, Y. Huang, J. Zhang, D. Zhang, J. Liu, Q. Liu, H. Lin and X. Yu, *Sci. China. Chem.*, 2011, **54**, 129–136.
16 Q.-L. Li, J. Huang, Q. Wang, N. Jiang, C.-Q. Xia, H.-H. Lin, J. Wu and X.-Q. Yu, *Bioorg. Med. Chem.*, 2006, **14**, 4151–4157.
17 K. P. Balakrishnan, T. A. Kaden, L. Siegfried and A. D. Zuberbühler, *Helv. Chim. Acta*, 1984, **67**, 1060–1069.
18 T. L. Walker, S. Mula, W. Malasi, J. T. Engle, C. J. Ziegler, A. van der Est, J. Modarelli and M. J. Taschner, *Dalton Trans.*, 2015, **44**, 20200–20206.
19 T. Rotärmel, J. Becker and S. Schindler, *Faraday Discuss.*, 2022, **234**, 70–85.
20 A. Johnson, L. Iffland-Mühlhaus, J. Northcote-Smith, K. Singh, F. Ortu, U.-P. Apfel and K. Suntharalingam, *Dalton Trans.*, 2022, **51**, 5904–5912.
21 M. W. Glenny, L. G. A. van de Water, J. M. Vere, A. J. Blake, C. Wilson, W. L. Driessen, J. Reedijk and M. Schröder, *Polyhedron*, 2006, **25**, 599–612.
22 A. H. Alberts, J.-M. Lehn and D. Parker, *J. Chem. Soc., Dalton Trans.*, 1985, 2311–2317.
23 S. Afshar, S. T. Marcus, L. R. Gahan and T. W. Hambley, *Aust. J. Chem.*, 1999, **52**, 1–6.
24 M. M. Bernardo, R. R. Schroeder and D. B. Rorabacher, *Inorg. Chem.*, 1991, **30**, 1241–1247.
25 K. B. Yatsimirskii and V. V. Pavlishchuk, *J. Coord. Chem.*, 1996, **37**, 341–348.
26 M. C. Styka, R. C. Smierciak, E. L. Blinn, R. E. DeSimone and J. V. Passariello, *Inorg. Chem.*, 1978, **17**, 82–86.
27 B. M. Gatehouse, S. E. Livingstone and R. S. Nyholm, *J. Chem. Soc.*, 1957, 4222–4225.

28 R. Clay, P. Murray-Rust and J. Murray-Rust, *Acta Cryst.*, 1979, **B35**, 1894–1895.
29 J. Nagaj, K. Stokowa-Sołtys, E. Kurowska, T. Frączyk, M. Jeżowska-Bojczuk and W. Bal, *Inorg. Chem.*, 2013, **52**, 13927–13933.
30 L. Guilloreau, S. Combalbert, A. Sournia-Saquet, H. Mazarguil and P. Faller, *ChemBioChem*, 2007, **8**, 1317–1325.
31 E. L. Hegg and J. N. Burstyn, *Inorg. Chem.*, 1996, **35**, 7474–7481.
32 A. Sreedhara, J. D. Freed and J. A. Cowan, *J. Am. Chem. Soc.*, 2000, **122**, 8814–8824.
33 Y. W. Lee, M. S. Ha and Y. K. Kim, *Neurochem. Res.*, 2001, **26**, 1187–1193.
34 J. Hormann, S. Streller and N. Kulak, *J. Chem. Educ.*, 2018, **95**, 1848–1855.
35 B. Tang, L. Zhang and Y. Geng, *Talanta*, 2005, **65**, 769–775.
36 H. Maeda, Y. Fukuyasu, S. Yoshida, M. Fukuda, K. Saeki, H. Matsuno, Y. Yamauchi, K. Yoshida, K. Hirata and K. Miyamoto, *Angew. Chem. Int. Ed.*, 2004, **43**, 2389–2391.
37 K. P. Balakrishnan, T. A. Kaden and A. D. Zuberbühler, *Inorg. Chim. Acta*, 1983, **79**, 202–203.
38 J. C. Joyner, J. Reichfield and J. A. Cowan, *J. Am. Chem. Soc.*, 2011, **133**, 15613–15626.
39 P. de Hoog, M. J. Louwerse, P. Gamez, M. Pitié, E. J. Baerends, B. Meunier and J. Reedijk, *Eur. J. Inorg. Chem.*, 2008, 612–619.
40 H. Gao, Z. Ke, N. J. DeYonker, J. Wang, H. Xu, Z.-W. Mao, D. L. Phillips and C. Zhao, *J. Am. Chem. Soc.*, 2011, **133**, 2904–2915.
41 X. Zhang, X. Liu, D. L. Phillips and C. Zhao, *ACS Catal.*, 2016, **6**, 248–257.
42 T. Miao, Q. Deng, H. Gao, X. Fu and S. Li, *J. Chem. Inf. Model.*, 2018, **58**, 859–866.
43 L. E. Roy, E. Jakubikova, M. G. Guthrie and E. R. Batista, *J. Phys. Chem. A*, 2009, **113**, 6745–6750.
44 M. D. Liptak and G. C. Shields, *J. Am. Chem. Soc.*, 2001, **123**, 7314–7319.
45 M. D. Liptak, K. C. Gross, P. G. Seybold, S. Feldgus and G. C. Shields, *J. Am. Chem. Soc.*, 2002, **124**, 6421–6427.
46 K. Paraskevopoulos, M. Sundararajan, R. Surendran, M. A. Hough, R. R. Eady, I. H. Hillier and S. S. Hasnain, *Dalton Trans.*, 2006, 3067–3076.
47 L. M. P. Lima, D. Esteban-Gómez, R. Delgado, C. Platas-Iglesias and R. Tripier, *Inorg. Chem.*, 2012, **51**, 6916–6927.
48 R. P. Hertzberg and P. B. Dervan, *Biochemistry*, 1984, **23**, 3934–3945.
49 A. D. Becke, *J. Chem. Phys.*, 1993, **98**, 5648–5652.
50 C. Lee, W. Yang and R. G. Parr, *Phys. Rev. B.*, 1988, **37**, 785–789.
51 M. J. Frisch, G. W. Trucks, H. B. Schlegel, G. E. Scuseria, M. A. Robb, J. R. Cheeseman, G. Scalmani, V. Barone, B. Mennucci, G. A. Petersson, H. Nakatsuji, M. Caricato, X. Li, H. P. Hratchian, A. F. Izmaylov, J. Bloino, G. Zheng, J. L. Sonnenberg, M. Hada, M. Ehara, K. Toyota, R. Fukuda, J. Hasegawa, M. Ishida, T. Nakajima, Y. Honda, O. Kitao, H. Nakai, T. Vreven, J. A. Montgomery, J. E. Peralta, F. Ogliaro, M. Bearpark, J. J. Heyd, E. Brothers, K. N. Kudin, V. N. Staroverov, R. Kobayashi, J. Normand, K. Raghavachari, A. Rendell, J. C. Burant, S. S. Iyengar, J. Tomasi, M. Cossi, N. Rega, M. J. Millam, M. Klene, J. E. Knox, J. B. Cross, V. Bakken, C. Adamo, J. Jaramillo, R. Gomperts, R. E. Stratmann, O. Yazyev, A. J. Austin, R. Cammi, C. Pomelli, J. W. Ochterski, R. L. Martin, K. Morokuma, V. G. Zakrzewski, G. A. Voth, P. Salvador, J. J. Dannenberg, S. Dapprich, A. D. Daniels, O. Farkas, J. B. Foresman, J. V. Ortiz, J. Cioslowski and D. J. Fox, *Gaussian 09, Revision D.01*, Gaussian,Inc., Wallingford CT, 2009.
52 P. J. Hay and W. R. Wadt, *J. Chem. Phys.*, 1985, **82**, 299–310.
53 C. Gonzalez and H. B. Schlegel, *J. Phys. Chem.*, 1990, **94**, 5523–5527.
54 C. Gonzalez and H. B. Schlegel, *J. Chem. Phys.*, 1989, **90**, 2154–2161.
55 M. Dolg, U. Wedig, H. Stoll and H. Preuss, *J. Chem. Phys.*, 1987, **86**, 866–872.
56 A. V. Marenich, C. J. Cramer and D. G. Truhlar, *J. Phys. Chem. B*, 2009, **113**, 4538–4543.
57 S. Grimme, J. Antony, S. Ehrlich and H. Krieg, *J. Chem. Phys.*, 2010, **132**, 154104.
58 J. Schnödt, M. Sieger, B. Sarkar, J. Fiedler, J. S. Manzur, C.-Y. Su and W. Kaim, *Z. Anorg. Allg. Chem.*, 2011, **637**, 930–934.
59 S. Stoll, and A. Schweiger, *J. Magn. Reson.*, 2006, **178**, 42–55.